Materials and Design 132 (2017) 505–511

Contents lists available at ScienceDirect

Materials and Design

journal homepage: www.elsevier.com/locate/matdes

A photochemical approach for preparing graphene and fabrication of SU-8/graphene composite conductive micropatterns

Bing Xue [a], Yingquan Zou [a,*], Yuchun Yang [b]

[a] Chollege of Chemistry, Beijing Normal University, Beijing 100875, China
[b] Shenzhen Rongda Photosensitive Science & Technology Co., Ltd., Shenzhen 518103, China

HIGHLIGHTS

- A metal-free photochemical reduction method towards graphene oxide is proposed.
- The mechanism relies on free-radical reduction and oxygen inhibition elimination.
- High electrical conductivity is obtained via removing oxygen containing groups.
- SU-8/graphene composite shows a facile processability on various substrates.

GRAPHICAL ABSTRACT

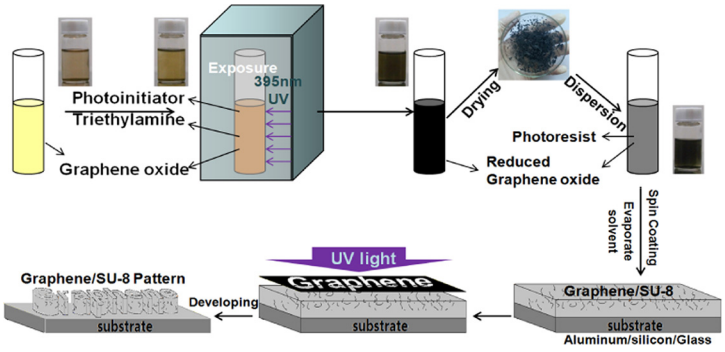

ARTICLE INFO

Article history:
Received 8 March 2017
Received in revised form 17 July 2017
Accepted 18 July 2017
Available online 19 July 2017

Keywords:
Photoinitiator
UV-irradiation
Reduced graphene oxide
SU-8 photoresist
Photolithography

ABSTRACT

We proposed herein a facile, fast and low cost metal-free photochemical method for preparing reduced graphene oxide (rGO) by ultraviolet (UV) irradiation of a solution containing mixture of a photoinitiator such as phenylbis(2,4,6-trimethylbenzoyl)phosphine oxide (GR-XBPO) and a triethylamine (TEA) in ethanol. Free radicals are generated via photoinitiator decomposition under UV irradiation. In this process, graphene oxide (GO) rapidly reduced to graphene via extensively removal of oxygen-containing functional groups (OFGs) by free radicals in the presence of anti-oxide inhibitor such as TEA exists. Furthermore, we prepared flexible conductive micropatterns over rGO/SU-8 composites deposited on several substrates (e.g., glass, polyethylene terephthalate (PET), aluminum, and silicon) by dispersing rGO into a photocurable SU-8 resin by means of a photolithography technique. The incorporation of rGO changed the properties of the composites. Thus, the behavior of SU-8 resin shifted from insulating to conductive/antistatic upon incorporation of rGO nanocomposites. This preliminary study provides us with the opportunity to not only develop an efficient metal-free photochemical reduction route towards GO but also obtain a processable conductive micropattern by optimizing the overall processing parameters, and maximizing the advantages of them for future carbon-based nanocomposites at large scale.

1. Introduction

The development of graphene-based materials has received a strong interest in recent years owing to the unique optical, electrical, thermal, and mechanical properties [1–4] and advanced and varied applications (e.g., energy storage, sensors, composites, semiconductors, and electrodes) of this material [5–11]. However, high-yield effective synthesis processes have to be developed before graphene-based materials can be successfully utilized in these fields [12]. Thus, graphene production has been intensively explored since its discovery [13]. Up to now, the main scalable and low cost route for graphene production is the two-

* Corresponding author.
E-mail addresses: xuebing_btbu@126.com (B. Xue), zouyq@263.net (Y. Zou).

http://dx.doi.org/10.1016/j.matdes.2017.07.034
0264-1275/

step chemical/reduction approach [14]. This method offers potential scalability, impressive conversion efficiency, and superior processability, and several chemical methods have been performed under a variety of conditions [15]. Among them, a mild, high efficiency, low cost, simple and environmentally friendly method such as photochemical reduction has been used to prepare copper, silver, and gold nanoparticles [16–18]. The photochemical synthesis of metal nanoparticles allows controlling the rate of nanoparticle formation. Following the same idea, some works about GO reduction by this photochemical reaction with the assistance of a photocatalyst like TiO_2 [19–22], ZnO [23] and $BiVO_4$ [24] have been reported. However, the reduction with metal-free photocatalyst has been scarcely used, especially by a photoinitiator to prepare high conductive graphene materials.

Photolithography has been considered as a standard patterning method for decades owing to its well established procedures and particular characteristics (e.g., environmentally friendly, fast, and energy saving, among others) [25]. Furthermore, it is also a scalable and continuous micro/nanofabrication method of three-dimensional (3D) structures that has been proven to be an efficient approach for the development of micro- and nano-technologies [26,27]. Thus, under uniform illumination, a certain prepared pattern is transferred from a photomask to the light-sensitive photoresist material. Nanocomposite fillers allow providing the matrix with valuable properties such as electrostatic discharge, high mechanical performance, large operating temperature range, and chemical resistance, among others [28]. However, one of the most important factors influencing the properties of nanocomposites involves the uniform dispersion of the nanofiller into polymer matrix [8,9,29]. Recently, graphene has been proposed as filler, despite pristine graphene is prone to form irreversible agglomerates through van der Waals interactions [30–32]. Moreover, the structure of graphene is atomically smooth and lacks interfacial bonding [33]. In contrast, rGO nanoplates possess functional groups and are advantageous in that they can be added to the polymeric matrix [34].

Herein we propose a new facile method for obtaining graphene via photochemical reduction of GO using a photoinitiator. This graphene product was successfully added to a photoresist to form conductive flexible patterns on various substrates (e.g., glass, aluminum, silicon, and PET, among others), thereby rendering the substrate with new characteristics and potential applications in surface coating, smart window, and simple conductive devices, among others [35]. GR-XBPO is a free radical type photoinitiator commonly used in photoresists, while also showing high efficiency and weather fastness characteristics. We also demonstrated that photoinitiator alone can hardly reduce GO. Thus, TEA is an essential part in this process, serving as an anti-oxide inhibitor, and the reduction mechanism was explored. Furthermore, the final graphene product was used as a filler to prepare flexible patterns on various substrates via a photolithography technique, which is a critical step in bring these excellent materials to practical applications. The SU-8 epoxy-based resin is extensively employed in microfluidic and micro-optics devices because of its good mechanical, thermo-mechanical, chemical resistance and biocompatibility properties [36–38]. In addition to carbon-based nanofillers such as carbon-nanotubes(CNTs), graphene can largely improve the electrical and thermal conductivities of polymer composites owing to its unique nanostructure and superior properties [39,40]. The planar structure of graphene can provide a 2 D path for phonon transport, which in favor of the fabrication of graphene nanodevices, nanoscale graphene transistors and single electron transistors [41,42]. Additionally, the presence of residual epoxy reactive groups on the platelets of rGO allows proper binding between the conductive filler and the polymeric matrix, and the high surface area can enhance the electrical conductivity [27,31,33,34]. This article provides a paradigm for the photochemical production of graphene while also developing graphene-based materials by using this as a filler. We anticipate that this work can pay the way for the development of new electrical products while also allowing the development of carbon-based devices at large scale.

2. Experimental

2.1. Starting materials

Graphite powder (325 mesh) was purchased from Qingdao HuaTai Co, Ltd. SU-8 2050 photoresist and developer (Propylene Glycol Monomethyl Ether Acetate, PGMEA) were purchased from MicroChem, USA. Sodium nitrate (99.5%), potassium permanganate (99%), concentrated sulphuric acid (98%), concentrated hydrochloric acid (A.R.), ethanol (A.R.) and 30% H_2O_2 aqueous solutions were analytical-grade and obtained from Beijing Chemical Reagents Company. All chemical reagents were used without any further purification, and all the experiments were completed in our lab.

2.2. Preparation of GO and rGO

GO was prepared according to the procedure described by Hummers and Offeman [43]. In the case of rGO, a reactive solution was prepared by mixing GO (4 mg), photoinitiator GR-XBPO (60 mg), TEA (4 mL) and ethanol (20 mL) in a transparent test tube. The suspension was irradiated with a 395 nm UV light source placed at a distance of 10 cm, for 10 min at ambient temperature in a dark environment. The radiation intensity of the 395 nm UV light source is 100 mW/cm^2. The radiation intensity was measured with an actinometer built by the Photoelectric Instrument Factory of Beijing Normal University. The final rGO was obtained by centrifugation of the black precipitate, washed with ethanol three times, dried at 65 °C for 5 h, and finally characterized.

2.3. Fabrication of rGO/SU-8 pattern

The as-obtained rGO was dispersed in ethanol and ultrasonicated for 10 min. The resultant suspension was subsequently added to the SU-8 photoresist. After 20 min of stirring in a beaker at 50 °C, a rGO sheet was uniformly dispersed in the SU-8 photoresist. SU-8 is a negative tone photoresist, and the patterned structures were prepared by the following process. First, the substrate (e.g., polyethylene terephthalate (PET), glass, aluminum, and silicon) was ultrasonically cleaned with isopropyl alcohol and dried with a purified nitrogen stream. The substrate was subsequently pre-baked at 95 °C for 10 min in a convection oven to remove potential moisture and contaminant traces. A typical spinning process for preparing SU-8 photoresist films on substrate was carried out (800 rpm for 10 s, then 1200 rpm for 60 s) on a SC-1B spin coater, followed by 65 °C (10 min) and 95 °C (30 min) soft bake processes. Next, the photoresist bearing a patterning mask was UV exposed on an Oriel exposure tool (light intensity: 360 mJ/cm^2) for ca. 6 min. The exposed photoresist samples were subsequently subjected to a post-exposure bake (PEB) for 30 min at 95 °C. The development process was carried out on an SU-8 developer from MicroChem (SU-8 Developer) to get rid of the unwanted SU-8 coverage.

2.4. Characterizations

The structure of the samples was analyzed on a Shimadzu X-ray diffraction (XRD) device model XRD-6000 (Cu Kα radiation, 1.5406 Å). The quality and structure of the GO and rGO layers were further characterized by Fourier transform infrared spectroscopy (FTIR) on an IRAffinity-1/Shimadzu spectrometer) in the 400–4000 cm^{-1} range, operating in the transmission mode. The samples were further characterized by X-ray photoelectron spectroscopy (XPS, ESCSLAB 250Xi/ThermoFisher) and by Raman spectroscopy (LabRAM Aramis/Horiba Jobin Yvon). The UV–Vis spectra were acquired on a PerkinElmer-LS55 instrument in the 200–700 nm range.

The morphologies of the GO and rGO films were characterized by scanning electron microscopy (SEM, S-4800/Hitachi) without any pretreatment. Transmission electron microscopy (TEM) imaging and electron diffraction were conducted on a TF 20 microscope. The TEM

samples for TEM analysis were prepared by ultrasonication at 20 W for 10 min, with 10 μL of the supernatant being dropped onto the holey carbon grids.

The conductivities were measured by a four-point method on a thin glass sheet (22 mm × 22 mm). A picoampere meter (Keithley 2000, bench digital multimeter, 6–1/2-Digit DMM), and a four-point probe ST2558B-F01S (Suzhou Jingge Electronic Co., Ltd. China) were connected to measure the DC conductivity. The rGO films on glass sheet were prepared by following the procedure described in Fig. S7 (supporting information).

3. Results and discussion

3.1. Preparation, SEM and TEM analysis of rGO sheets

The synthesis of GO has been widely studied via the Hummers method which is accompanied by overoxidation and the formation of lattice defects. Various approaches have been proposed so far to perform the reduction of GO, although they are time-consuming and complex. Herein, we propose a time-saving, simple method to reduce GO. Before the reduction experiment, UV–Vis absorption spectra of GR-XBPO in ethanol were obtained to ensure proper absorption of the material at the selected UV light wavelength (Fig. S1). Subsequently, we investigated the photoreduction of GO. rGO was easily obtained by irradiating the GO ethanol mixture solution (0.2 mg/mL, 20 mL) containing GR-XBPO (60 mg) and TEA (4 mL) with 395-LED UV light. After 10 min of irradiation, the yellow suspension became black and subsequently deposited (Fig. 1a). The dried rGO sheets are displayed in Fig. 1b, while their structures as revealed by SEM are shown in Fig. 1c-e. Fig. 1f shows a TEM image of the rGO products and the selected area electron diffraction (SAED) pattern (inset of Fig. 1f) showed the typical hexagonal honeycomb structure of graphene with hexagonal and symmetrical spots, thereby confirming the formation of graphene.

3.2. XPS, Raman, FTIR and XRD characterizations of GO and rGO

The XPS spectrum provides surface elemental compositions of materials. The survey scans before and after irradiation were obtained (Fig. 2a). The UV irradiation process resulted in higher C:O ratios, thereby demonstrating that GR-XBPO reduced GO by decreasing the amount of OFGs. However, TEA (GO_{TEA}) alone did not induce reduction, thereby indicating that GR-XBPO is an essential part within the reduction process (Fig. 2, middle line). High resolution XPS core level analysis was also performed on the C1s spectrum (see C1s inset of Fig. 2a). The C1s spectrum of GO showed three peaks corresponding to C═C (284.3 eV), C—O (286.8 eV) and C═O (288.5 eV) species. The C═O component nearly disappeared and the intensity of C—O largely weakened after the UV treatment. The Raman spectrum reflected the quality of the sample. Thus, higher $I_{D(1350\ cm^{-1})}$ / $I_{G(1590\ cm^{-1})}$ ratios after reduction revealing larger concentrations of localized sp^3 defects, and sp^2 domains with lower average sizes (Fig. 2b) [44–47]. As shown in the FTIR spectrum (Fig. 2c), the characteristic stretching vibrations of GO were almost removed as a result of the deoxygenating process. The minor amount of OFGs present in rGO (as detected by FTIR) were indicative of the successful synthesis of this material by the UV-assisted method proposed herein. The XRD patterns of GO and rGO are shown in Fig. 2d. The peak corresponding to the (002) plane shifted from 11.24° ($d = 0.787$ nm) for GO to 23.58° ($d = 0.377$ nm) after the UV-assisted reduction. This reduction in the planar interspace was indicative of the removal of OFGs in large amounts. However, this distance was still larger than that of natural graphite ($d = 0.334$ nm), indicating that the regular crystallinity of graphite was damaged [48]. As indicated

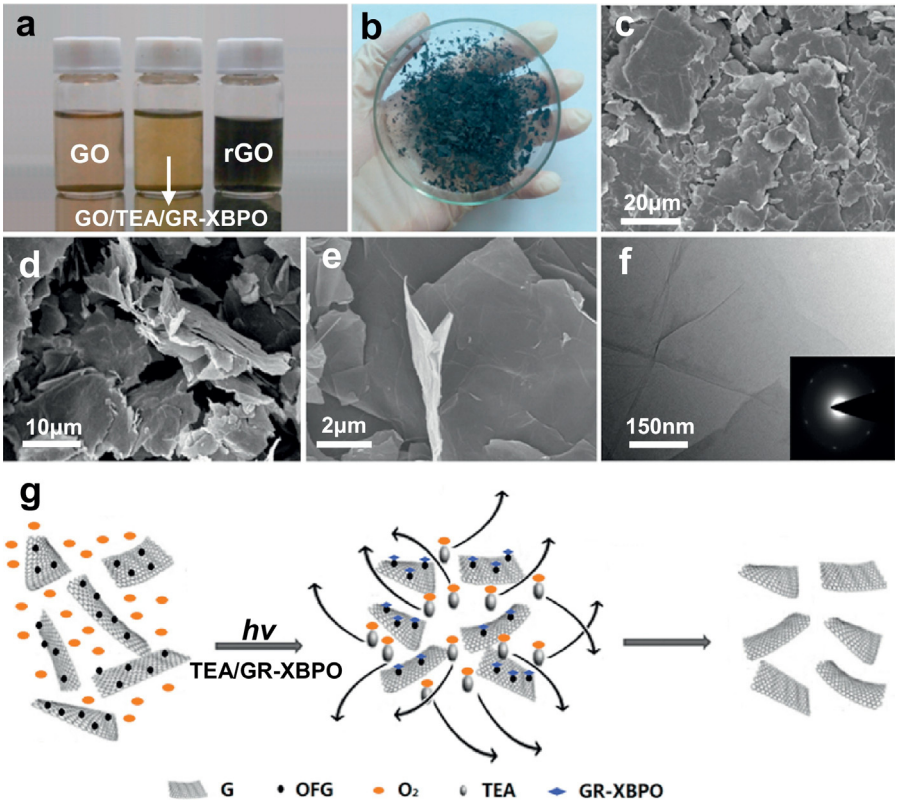

Fig. 1. a) Photographs of GO, the GO/TEA/GR-XBPO suspension and the mixture irradiated for 10 min upon 395 nm LED light. b) Dried rGO sheets. c–e) SEM images of rGO at different magnifications. f) TEM image of rGO sheets. The inset depicts the SAED image of rGO. g) Schematic illustration of the process followed for the synthesis of rGO.

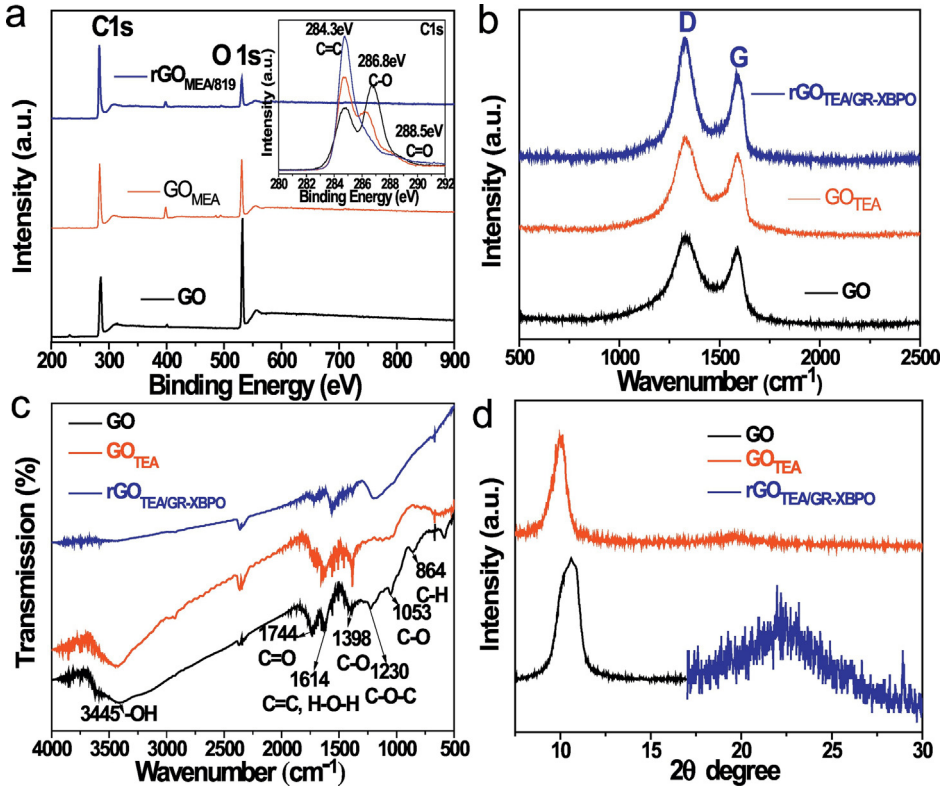

Fig. 2. Characterizations of GO, GO_{TEA}, and rGO. a) XPS survey spectra. The inset shows the C1s spectra of GO, GO_{TEA}, and rGO. b) Raman spectra. c) FTIR spectra. d) XRD patterns of GO, GO_{TEA}, and rGO.

above, TEA alone was not able to induce this reduction (upside curve in Fig. 2d). This flexible and highly efficient technique is versatile and scalable for mass production of rGO. The rGO product can be produced at large scale by enlarging the reaction system (Fig. S2). On the basis of these experimental observations, the reactive process of rGO is illustrated in Fig. 1g and S3.

3.3. Photoreaction process analysis

The UV–Vis spectra photoreaction mixture while changing both the reaction time and the GR-XBPO loading are presented in Fig. 3. As shown in Fig. 3a, the absorbance of GR-XBPO decreased with the irradiation time as a result of its decomposition in ethanol upon UV irradiation. The inset of Fig. 3a shows the colors of the suspensions obtained after different irradiating times (i.e., 0, 10, 40, 120, and 160 s). As reported, oxygen inhibition is an inevitable phenomenon when polymerizing under ambient environment, and several methods have been developed to overcome oxygen inhibition (e.g., utilization of additives consuming oxygen within the reactive system) one of the approaches is using another additives to consume oxygen in the reactive system [49]. Primary, secondary, and tertiary amines can all be used as hydrogen donors, although tertiary amines are preferred owing to their lower volatility and higher oxygen-consuming activity. Herein, tertiary amines were used to ensure UV-assisted reduction to proceed readily. Since amines could consume O_2, the performance of the active free radicals was highly increased as a result. Moreover, once irradiation was finished, rGO flocks floated on the reaction solution within the first 60 s and slowly sank up to 540 s, after which they were deposited on the bottom. This phenomenon can be explained by the low amounts of OFGs remaining on the surface of the rGO flocks and it is described in Fig. S4. Fig. 3b displays the absorption spectra of GO and GR-XBPO (60 mg) suspensions in ethanol at different GO content (4, 8, 12, 16, and 20 mL, of a

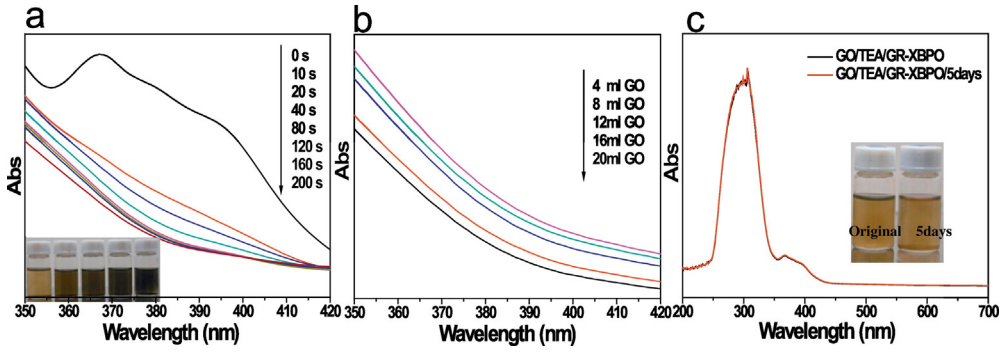

Fig. 3. a) Absorption spectra and pictures of a GO/GR-XBPO dispersion in an ethanol/TEA solution after different irradiation times. The inset shows pictures of the suspension after different irradiating times (0, 10, 40, 120, and 160 s). b) Absorption spectra of a solution (20 mL of ethanol, 4 mL of TEA, and 60 mg of GR-XBPO) at different GO loadings (4, 8, 12, 16, and 20 mL of a 0.2 mg/mL solution). c) UV–Vis spectra of the GO-ethanol solution containing GO/TEA/GR-XBPO kept in a dark environment for 5 days without irradiation. The inset shows the pictures of the suspensions: initial and after 5 days.

Table 1
Electrical properties of the rGO/SU-8 composites.

Samples	V/I (Ω)	Thickness Z_0 (cm)	Electrical resistivity ρ (Ω × cm)	Electrical conductivity σ (S/cm)
rGO	1.38×10^{-2}	1.65×10^{-2}	6.25×10^{-4}	9.70×10^{2}
SU-8	–	–	–	–
SU-8 + 1 wt% rGO	–	–	–	–
SU-8 + 2 wt% rGO	–	–	–	–
SU-8 + 3 wt% rGO	3.28×10^{2}	1.67×10^{-2}	2.48×10^{1}	4.03×10^{-2}
SU-8 + 4 wt% rGO	8.50×10^{1}	2.35×10^{-2}	2.00×10^{0}	5.00×10^{-1}

0.2 mg/mL solution) after UV irradiation for 10 min. The amount of electrons produced at the GR-XBPO surface and subsequently transferred to the GO platelets (triggering their reduction) increased with the GO loading. This photo-assisted GO reduction process is advantageous in that it is environmentally friendly while also being potentially modulated on demand by tuning the UV-irradiation. Moreover, a GO/GR-XBPO/TEA ethanol suspension kept in a dark environment for 5 days without irradiation showed nearly unchanged UV–Vis spectra and color as compared to the initial suspension. These data indicated that GO, GR-XBPO and UV-light are essential for the photoreduction process. Unlike other methods [50], this work provides a facile, scalable, and time-saving metal-free photochemical route for preparing rGO.

3.4. Preparation procedures of rGO/SU-8 films

The SU-8 photoresist is an important part of the micro-electronic-mechanical system (MEMS) technique that provides a new material platform for developing large area devices for various applications. When incorporated into nonconductive systems, graphene allows sheet to sheet interconnectivity thereby providing a conductive pathway through regions of nonconductive systems [51]. SU-8 photoresist would be largely used in integrated circuit and electromagnetic shielding applications (among others) provided it is accompanied with certain conductivity. Therefore, rGO was used herein as a filler of SU-8 photoresist and the conductive properties of the resulting rGO/SU-8 material were explored. At here, the further UV process of the photolithography did not chemically reduce the rGO more than its original state, because some of the work had demonstrated that free-radical photoinitiators producing free radicals have the ability to reduce metal ions [52,53], and we also confirmed this conclusion to reduce GO in our former reported work [50]. However, in this work, before UV curing, the soft bake step would evaporate nearly all the inner solvent of the photoresist, and no other solvents and photoinitiators used, therefore it is hardly to reduce the rGO again when absence these components in the photoresist. With the aim to understand the relationship between the rGO concentration and the conductivity of the material, different loadings of rGO (i.e., 1, 2, 3, and 4 wt%) were uniformly added to the SU-8 photoresist, and the corresponding photographs are shown in Fig. S5a. All the electrical characterization measurements carried out on a UV-cured coating over an insulating glass substrate (Fig. S5b, SU-8 + 4 wt% rGO). The magnified picture in Fig. S5c shows the low-transparent SU-8 + 4 wt% rGO thin film on a glass substrate.

3.5. Conductivity of rGO and rGO/SU-8 films

The conductivities of the rGO/SU-8 materials were measured by a four-point method on a thin glass sheet with a certain rGO/SU-8 coating thickness (see cross-section SEM images in Fig. S6). The conductivity was calculated by the following formulas:

$$\rho = V \cdot I^{-1} \cdot Z_0 \cdot F(s, x_0, y_0) \quad (1)$$

$$\sigma = 1/\rho \quad (2)$$

where ρ is the resistivity, V is the measured voltage, I is the applied current, $F(s, x_0, y_0)$ is the modified function ($F = 4.53$) [54], Z_0 is the film thickness, S is the probe spacing, x_0 (y_0) is the half width (length) of the rectangle sample, and σ is the conductivity.

The actual resistivity values calculated are listed in Table 1. As shown in Table 1, the resistivity decreased with the filler content (minimum resistivity of ca. 2.00×10^0 Ω × cm at a filler loading of 4 wt%). Therefore, the conductivity can be tuned by changing the concentration of the filler [55]. The SU-8 resins containing 1 and 2 wt% of rGO did not show any measurable electrical conductivity (i.e., the measurement was below the detection limit of the instrument). However, at higher rGO concentrations, the binder did not achieve a homogeneous crosslinking, which is in agreement with previous reports [27]. Fig. 4 represents repeated conductivity measurements, while the inset shows a schematic diagram of the four-point measurement.

The electrical conductivity of rGO is also listed in Table 1, while the film deposited on the glass sheet was formed via the route described in Supporting S7. Reduction is known to improve the electrical conductivity via removal of the OFGs and restoration of part of the aromatic nature of the bonding. Despite the structural defects and the presence of remaining OFGs on the graphene sheets after reduction, direct current (DC) conductive measurements on rGO showed higher conductivity values (9.70×10^2 S/cm) than most of the previous reported rGO samples (Table 1, Supporting Information). These results imply that larger amounts of charge transfer channels across the sample are presents and in-plane defects are not dominant factor in determining the conductivity [56].

3.6. Fabrication of rGO/SU-8 micropatterns on different substrates

Finally, rGO/SU-8 composites with high electrical conductivity can be tailored into patterned structures on various substrates (e.g., PET, silicon, and aluminum) for special applications. As shown in previous

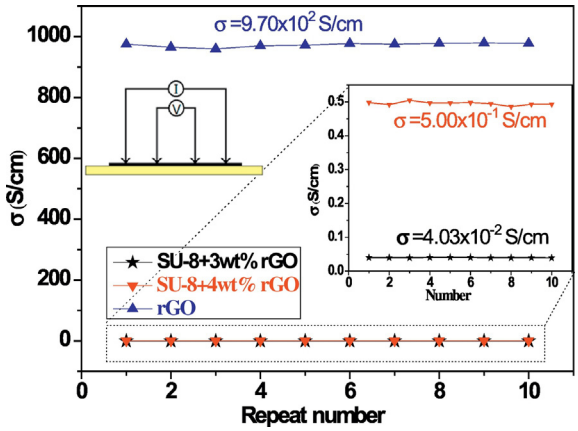

Fig. 4. Repeated conductivity measurements for the rGO, SU-8 + 3 wt% rGO, and SU-8 + 4 wt% rGO samples. The inset is the schematic diagram of the four-point measurement.

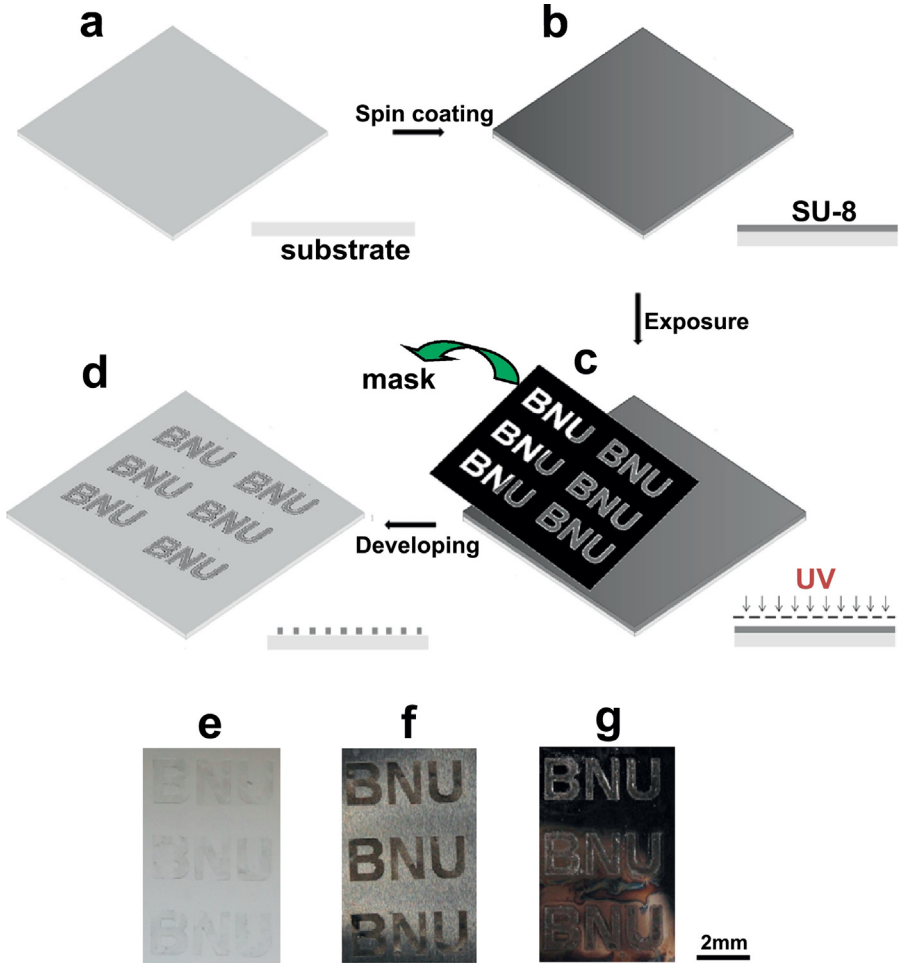

Fig. 5. a–d) Schematic illustration of the process for preparing rGO/SU-8 patterns. e–g) Pictures of the rGO/SU-8 patterns on PET, aluminum, and silicon substrates.

investigations [27], the addition of graphene to epoxy photocurable formulations led to a large decrease of the polymerization rate depending of the filler loading fraction. It is not difficult to understand that the flake-like graphene would shield a certain amount of UV light, thereby resulting in lower amounts of photogenerated reactive species and subsequently decreasing the rate of epoxy groups conversion. Therefore, with the aim to obtain integrated patterns on the substrate, it is very important to adjust the conditions during the photolithography process. Thus, flexible patterns on different types of substrates were prepared.

A physical mask provided with a strip pattern was used to tune the patterned structure. The fabrication process of the strip pattern on the PET film based on rGO/SU-8 is illustrated step-by-step in Fig. 5a-d. First, a clear PET substrate was selected (Fig. 5a). Subsequently, the PET surface was spin coated with the rGO/SU-8 resist (Fig. 5b). The third step involved the utilization of a mask placed on the PET substrate (Fig. 5c). Subsequently, the mask was carefully removed after the develop process, and the patterned rGO/SU-8 were formed in the PET surface as a result (Fig. 5e). This process was not limited to PET. Aluminum and silicon wafers also worked well for patterning G/SU-8 as demonstrated in Fig. 5f-g. The patterns showed good adhesion features with the substrates.

4. Conclusions

In summary, rGO has been synthetized using a photoinitiator as a reductant by a facile, cheap, and scalable metal-free photochemical reduction method. The rGO platelets were uniformly dispersed in SU-8 resist and subsequently patterned on various substrates. Moreover, rGO served as a conductive filler and demonstrated high efficiency in improving the electrical conductivity through the polymer composite. Remarkably, the rGO/SU-8 material developed herein provides a new platform for developing specifically and arbitrarily tailorable graphene architectures at the micro and macroscopic scales, paving the way for versatile manipulation of graphene for advanced applications.

Appendix A. Supplementary data

Supplementary data to this article can be found online at http://dx.doi.org/10.1016/j.matdes.2017.07.034.

References

[1] D.R. Dreyer, S. Park, C.W. Bielawski, R.S. Ruoff, The chemistry of graphene oxide, Chem. Soc. Rev. 39 (2010) 228–240.
[2] X. Miao, S. Tongay, M.K. Petterson, K. Berke, A.G. Rinzler, B.R. Appleton, A.F. Hebard, High efficiency graphene solar cells by chemical doping, Nano Lett. 12 (2012) 2745–2750.
[3] H. Gwon, H.S. Kim, K.U. Lee, D.H. Seo, Y.C. Park, Y.S. Lee, B.T. Ahn, K. Kang, Flexible energy storage devices based on graphene paper, Energy Environ. Sci. 4 (2011) 1277–1283.
[4] E. Moralesnarváez, L. Baptistapires, A. Zamoragálvez, A. Merkoçi, A graphene-based biosensors: going simple, Adv. Mater. 29 (2017) 1604905.
[5] E.J. Yoo, J. Kim, E. Hosono, H.S. Zhou, T. Kudo, I. Honma, Large reversible Li storage of graphene nanosheet families for use in rechargeable lithium ion batteries, Nano Lett. 8 (2008) 2277–2282.
[6] C. Wang, Y. Li, Y. Zhu, X. Zhou, Q. Lin, M. He, High-κ solid-gate transistor configured graphene biosensor with fully integrated structure and enhanced sensitivity, Adv. Funct. Mater. 26 (2016) 7668–7678.
[7] W. Fu, L. Jiang, E.P. Van Geest, L.M.C. Lima, G.F. Schneider, Sensing at the surface of graphene field-effect transistors, Adv. Mater. 29 (2017) 1603610.

[8] S. Stankovich, D.A. Dikin, G.H.B. Dommett, K.M. Kohlhaas, E.J. Zimney, E.A. Stach, Graphene-based composite materials, Nature 442 (2006) 282–286.
[9] T. Ramanathan, A.A. Abdala, S. Stankovich, D.A. Dikin, M.H. Alonso, R.D. Piner, D.H. Adamson, H.C. Schniepp, Functionalized graphene sheets for polymer nanocomposites, Nat. Nanotechnol. 3 (2008) 327–331.
[10] K.S. Novoselov, A.K. Geim, S.V. Morozov, D. Jiang, Y. Zhang, S.V. Dubonos, I.V. Grigorieva, A.A. Firsov, Electric field effect in atomically thin carbon films, Science 306 (2004) 666–669.
[11] X. Wang, L.J. Zhi, N. Tsao, Z. Tomovic, J.L. Li, K. Mullen, Transparent carbon films as electrodes in organic solar cells, Angew. Chem. Int. Ed. 47 (2008) 2990–2992.
[12] Y.L. Zhong, Z. Tian, G.P. Simon, D. Li, Scalable production of graphene via wet chemistry: progress and challenges, Mater. Today 18 (2015) 73–78.
[13] M. Buzaglo, I.P. Bar, M. Varenik, L. Shunak, S. Pevzner, O. Regev, Graphite-to-graphene: total conversion, Adv. Mater. 29 (2017) 1603528.
[14] C. Li, X. Zhang, K. Wang, X. Sun, G. Liu, J. Li, H. Tian, J. Li, Y. Ma, Scalable self-propagating high-temperature synthesis of graphene for supercapacitors with superior power density and cyclic stability, Adv. Mater. 29 (2017) 1604690.
[15] C.K. Chua, M. Pumera, Chemical reduction of graphene oxide: a synthetic chemistry viewpoint, Chem. Soc. Rev. 43 (2014) 291.
[16] T. Itakura, K. Torigoe, K. Esumi, Preparation and characterization of ultrafine metal particles in ethanol by UV irradiation using a photoinitiator, Langmuir 11 (1995) 4129–4134.
[17] X. Zhu, B. Wang, F. Shi, J. Nie, Direct, rapid, facile photochemical method for preparing copper nanoparticles and copper patterns, Langmuir 28 (2012) 14461–14469.
[18] K.L. Mcgilvray, C. Fasciani, C.J. Buenoalejo, Photochemical strategies for the seed-mediated growth of gold and gold-silver nanoparticles, Langmuir 28 (2012) 16148–16155.
[19] O. Akhavan, M. Abdolahad, A. Esfandiar, M. Mohatashamifar, Photodegradation of graphene oxide sheets by TiO_2 nanoparticles after a photocatalytic reduction, J. Phys. Chem. C 114 (2010) 12955–12959.
[20] G. Williams, B. Seger, P.V. Kamat, TiO_2-graphene nanocomposites UV-assisted photocatalytic reduction of graphene oxide, ACS Nano 2 (2008) 1487–1491.
[21] L. Guardia, S. Villar-Rodil, J.I. Paredes, R. Rozada, A. Martínez-Alonso, J.M.D. Tascón, UV light exposure of aqueous graphene oxide suspensions to promote their direct reduction, formation of graphene-metal nanoparticle hybrids and dye degradation, Carbon 50 (2012) 1014–1024.
[22] S.R. Kim, M.K. Parvez, M. Chhowalla, UV-reduction of graphene oxide and its application as an interfacial layer to reduce the back-transport reactions in dye-sensitized solar cells, Chem. Phys. Lett. 483 (2009) 124–127.
[23] G. Williams, P.V. Kamat, Graphene-semiconductor nanocomposites: excited-state interactions between ZnO nanoparticles and graphene oxide, Langmuir 25 (2009) 13869–13873.
[24] Y.H. Ng, A. Iwase, A. Kudo, R. Amal, Reducing graphene oxide on a visible-light $BiVO_4$ photocatalyst for an enhanced photoelectrochemical water splitting, J. Phys. Chem. Lett. 1 (2010) 2607–2612.
[25] W. Qiao, W. Huang, Y. Liu, X. Li, L.S. Chen, J.X. Tang, Toward scalable flexible nanomanufacturing for photonic structures and devices, Adv. Mater. 28 (2016) 10353–10380.
[26] V. Penmatsa, T. Kim, M. Beidaghi, H. Kawarada, L. Gu, Z. Wang, C. Wang, Three-dimensional graphene nanosheet encrusted carbon micropillar arrays for electrochemical sensing, Nanoscale 4 (2012) 3673–3678.
[27] M. Sangermanoa, L. Calvara, E. Chiavazzo, L. Ventola, P. Asinari, V. Mittal, R. Rizzoli, L. Ortolani, V. Morandi, Enhancement of electrical and thermal conductivity of SU-8 photocrosslinked coatings containing graphene, Prog. Org. Coat. 86 (2015) 143–146.
[28] J. Leng, A.K.T. Lau, Multifunctional polymer nanocomposites, CRC Press Time (2011) 7–14.
[29] M.A.S. Sadigha, G. Marami, Investigating the effects of reduced graphene oxide additive on the tensile strength of adhesively bonded joints at different extension rates, Mater. Des. 92 (2016) 36–43.
[30] X. Sun, H. Sun, H. Li, H. Peng, Developing polymer composite materials: carbon nanotubes or graphene? Adv. Mater. 25 (2013) 5153–5176.
[31] X. Huang, X.Y. Qi, F. Boey, H. Zhang, Graphene-based composites, Chem. Soc. Rev. 41 (2012) 666–686.
[32] M. Drozdova, I. Hussainova, D. Pérez-Coll, M. Aghayan, R. Ivanov, M.A. Rodríguez, A novel approach to electroconductive ceramics filled by graphene covered nanofibers, Mater. Des. 90 (2016) 291–298.
[33] R. Verdejo, M.M. Bernal, L.J. Romasanta, Graphene filled polymer nanocomposites, J. Mater. Chem. 21 (2011) 3301–3310.
[34] T.K.B. Sharmila, J.V. Antony, M.P. Jayaknishnan, P.M.S. Beegum, E.T. Thachil, Mechanical, thermal and dielectric properties of hybride composites of epoxy and reduced graphene oxide/iron oxide, Mater. Des. 90 (2016) 66–75.
[35] J. Sun, Y. Chen, M.K. Priydarshi, T. Gao, X. Song, Y. Zhang, Z. Liu, Graphene glass from direct CVD routes: production and applications, Adv. Mater. 28 (2016) 10333–10339.
[36] A.D. Campo, C. Greimer, SU-8: a photoresist for high-aspect-ratio and 3D submicron lithography, J. Micromech. Microeng. 17 (2007) 81–95.
[37] B.A. Weisenberg, D.L. Mooradian, Hemocompatibility of materials used in microelectromechanical systems: platelet adhesion and morphology in vitro, J. Biomed. Mater. Res. 60 (2002) 283–291.
[38] P. Abgrall, A.M. Gué, Lab-on-chip technologies: making a microfluidic network and coupling it into a complete microsystem, J. Micromech. Mircoeng. 17 (2007) 15–49.
[39] M. Sangermano, S. Pegel, P. Pötschke, B. Voit, Antistatic epoxy coatings with carbon nanotubes obtained by cationic photopolymerization, Macromol. Rapid Commun. 29 (2008) 396–400.
[40] J.N. Coleman, U. Khan, Y.K. Gun'ko, Mechanical reinforcement of polymers using carbon nanotubes, Adv. Mater. 18 (2006) 689–706.
[41] N.S. Moghaddam, M.T. Ahmadi, J.F. Webb, M. Rahmani, H. Sadegi, M. Musavi, R. Ismail, Modeling of graphene nano-ribbon schottky diodes in the parabolic band structure limit, AIP Conf. Proc. 1499 (2012) 268–271.
[42] C. Stampfer, S. Fringes, J. Güttinger, F. Molitor, C. Volk, B. Terrés, J. Dauber, S. Engels, S. Schnez, A. Jacobsen, S. Dröscher, T. Ihn, K. Ensslin, Transport in graphene nanostructures, Front. Phys. 6 (2011) 271–293.
[43] W.S. Hummers, R.E. Offeman, Preparation of graphitic oxide, J. Am. Chem. Soc. 80 (1958) 1339.
[44] S. Stankovich, D.A. Dikin, R.D. Piner, K.A. Kohlhaas, A. Kleinhammes, Synthesis of graphene-based nanosheets via chemical reduction of exfoliated graphite oxide, Carbon 45 (2007) 1558–1565.
[45] S. Pei, H.M. Cheng, The reduction of graphene oxide, Carbon 50 (2012) 3210–3228.
[46] J. Gao, F. Liu, Y. Liu, N. Ma, Z. Wang, X. Zhang, Environment-friendly method to produce graphene that employs vitamin C and amino acid, Chem. Mater. 22 (2010) 2213–2218.
[47] F. Tuinstra, J.L. Koenig, Raman spectrum of graphite, J. Chem. Phys. 53 (1970) 1126–1130.
[48] W. Chen, L. Yan, P.R. Bangal, Preparation of graphene by the rapid and mild thermal reduction of graphene oxide induced by microwaves, Carbon 48 (2010) 1146–1152.
[49] S.C. Ligon, B. Husár, H. Wutzel, R. Holman, R. Liska, Strategies to reduce oxygen inhibition in photoinduced polymerization, Chem. Rev. 114 (2014) 557–589.
[50] B. Xue, Y. Zou, Y. Yang, UV-assisted reduction of graphite oxide to graphene by using a photoinitiator, J. Mater. Sci. 52 (2017) 4866–4877.
[51] S. Ansari, E.P. Giannelis, Functionalized graphene sheet-poly(vinylidene fluoride) conductive nanocomposites, J. Polym. Sci. B Polym. Phys. 47 (2009) 888–897.
[52] S. Giuffrida, G.G. Condorelli, L.L. Costanzo, I.L. Fragala, G. Ventimiglia, G. Vecchio, Photochemical mechanism of the formation of nanometer-sized copper by UV irradiation of ethanol bis(2,4-pentanedionato)copper(II) solutions, Chem. Mater. 16 (2004) 1260–1266.
[53] G.G. Condorelli, L.L. Costanzo, I.L. Fragala, S. Giuffrida, G. Ventimiglia, A single photochemical route for the formation of both copper nanoparticles and patterned nanostructured films, J. Mater. Chem. 13 (2003) 2409–2411.
[54] X. Geng, Y. Guo, D. Li, W. Li, C. Zhu, X. Wei, M. Chen, S. Gao, S. Qiu, Y. Gong, L. Wu, M. Long, M. Sun, G. Pan, L. Liu, Interlayer catalytic exfoliation realizing scalable production of large-size pristine few-layer gaphene, Sci Rep 3 (2013) 464–467.
[55] R.L. Whitby, Chemical control of graphene architecture: tailoring shape and properties, ACS Nano 8 (2014) 9733–9754.
[56] S. Stankovich, D.A. Dikin, R.D. Piner, K.A. Kohlhaas, A. Kleinhammes, Y. Jia, Y. Wu, S.T. Nguyen, R.S. Ruoff, Synthesis of graphene-based nanosheets via chemical reduction of exfoliated graphite oxide, Carbon 45 (2007) 1558–1565.